EBioMedicine 71 (2021) 103503

Contents lists available at ScienceDirect

EBioMedicine

journal homepage: www.elsevier.com/locate/ebiom

Research Paper

Reversing pathology in a preclinical model of Alzheimer's disease by hacking cerebrovascular neoangiogenesis with advanced cancer therapeutics

Chaahat S.B. Singh[a,b,c,d,g], Kyung Bok Choi[a,b,c,d,e,f,g], Lonna Munro[a,b,c,d,e,f,g], Hong Yue Wang[a,b], Cheryl G. Pfeifer[a,b,c,d,e,f,g], Wilfred A. Jefferies[a,b,c,d,e,f,g,h,*]

[a] Department of Medical Genetics, University of British Columbia, 2350 Health Sciences Mall, Vancouver, BC V6T 1Z4, Canada
[b] Michael Smith Laboratories, University of British Columbia, 2185 East Mall, Vancouver, BC V6T 1Z4, Canada
[c] Centre for Blood Research, University of British Columbia, 2350 Health Sciences Mall, Vancouver, BC V6T 1Z4, Canada
[d] The Djavad Mowafaghian Centre for Brain Health, University of British Columbia, 2215 Wesbrook Mall, Vancouver, BC V6T 1Z4, Canada
[e] Department of Microbiology and Immunology, University of British Columbia, 2350 Health Sciences Mall, Vancouver, BC V6T 1Z4, Canada
[f] Department of Zoology, University of British Columbia, 6270 University Blvd., Vancouver, BC V6T 1Z4, Canada
[g] The Vancouver Prostate Centre, Vancouver General Hospital, 2660 Oak Street, Vancouver, BC V6T 1Z4, Canada
[h] Department of Urologic Sciences, University of British Columbia, Gordon & Leslie Diamond Health Care Centre, Level 6, 2775 Laurel Street, Vancouver, BC V5Z 1M9, Canada

ARTICLE INFO

Article History:
Received 20 April 2020
Revised 28 June 2021
Accepted 13 July 2021
Available online xxx

Keywords:
Alzheimer's disease (AD)
Angiogenesis
Amyloid-beta (Aβ)
Axitinib
Blood-brain barrier (BBB)
Cognitive restoration
Anti-angiogenic drug treatment
Tg2576 mouse model

ABSTRACT

Background: Cognitive decline leading to dementia, accompanied by the accumulation of amyloid-beta (Aβ) in neuritic plaques together with the appearance of neurofibrillary tangles (NFT) composed of hyperphosphorylated tau protein (tau), are previously noted hallmarks of Alzheimer's disease (AD). We previously discovered hypervascularity in brain specimens from AD patients and consistent with this observation, we demonstrated that overexpression of Aβ drives cerebrovascular neoangiogenesis leading to hypervascularity and coincident tight-junction disruption and blood-brain barrier (BBB) leakiness in animal models of AD. We subsequently demonstrated that amyloid plaque burden and cerebrovascular pathogenesis subside when pro-angiogenic Aβ levels are reduced. Based on these data, we propose a paradigm of AD etiology where, as a compensatory response to impaired cerebral blood flow (CBF), Aβ triggers pathogenic cerebrovascular neoangiogenesis that underlies the conventional hallmarks of AD. Consequently, here we present evidence that repurposing anti-cancer drugs to modulate cerebrovascular neoangiogenesis, rather than directly targeting the amyloid cascade, may provide an effective treatment for AD and related vascular diseases of the brain.

Methods: We explored whether the anti-cancer drug, Axitinib, a small molecule tyrosine kinase inhibitor that targets vascular endothelial growth factor receptors (VEGFR) can inhibit aberrant cerebrovascular neoangiogenic changes, reduce Aβ deposits and reverse cognitive decline in an animal model of AD. One month post-treatment with Axitinib, we employed a battery of tests to assess cognition and memory in aged Tg2576 AD mice and used molecular analysis to demonstrate reduction of amyloid plaques, BBB leakage, hypervascularity and associated disease pathology.

Findings: Targeting the pro-angiogenic pathway in AD using the cancer drug, Axitinib, dramatically reduced cerebrovascular neoangiogenesis, restored BBB integrity, resolved tight-junction pathogenesis, diminishes Aβ depositions in plaques and effectively restores memory and cognitive performance in a preclinical mouse model of AD.

Interpretation: Modulation of neoangiogenesis, in an analogous approach to those used to treat aberrant vascularization in cancer and also in the wet form of age-related macular degeneration (AMD), provides an alternative therapeutic strategy for intervention in AD that warrants clinical investigation.

1. Introduction

Alzheimer's disease (AD) is a progressive neurological dementia that affects thinking, orientation and memory, causing impairment in

* Corresponding author at: Michael Smith Laboratories, University of British Columbia, 2185 East Mall, Vancouver, BC V6T 1Z4, Canada.
E-mail address: wilf@msl.ubc.ca (W.A. Jefferies).

https://doi.org/10.1016/j.ebiom.2021.103503

Research in context

Evidence before this study

AD is a progressive neurological dementia that affects thinking, orientation and memory, causing impairment in cognition, memory and social behaviour in over 50 million people worldwide. Emerging AD therapeutics based on current theories of disease pathogenesis involving Aβ and tau have been generally unsuccessful. However, cerebrovascular pathogenesis has recently gained wider acceptance as a hallmark feature of AD yet an under-investigated target for treating AD pathogenesis. For example, CAA is now recognized as a major pathological feature in the majority of AD cases and is a significant cause of cerebral microhemorrhages in the elderly. Related to these observations, our previous preclinical and clinical work and the research of others, indicate that BBB disruption occurs in the brains of AD patients and prior to Aβ plaque deposition in AD mouse models. Coincidently, pathogenic neoangiogenesis underlies BBB 'leakiness' that occurs in AD mouse models and can also be demonstrated in postmortem studies in the brains of AD patients. Halting or reversing cerebrovascular pathogenesis may therefore provide a new entry point for treating AD.

Added value of this study

Here we examine repurposing the anti-cancer drug, Axitinib, a VEGFR-specific angiogenesis inhibitor, to alleviate the cerebrovascular pathology in aged Swedish-familial AD Tg2576 model mice. We demonstrate that treatment with Axitinib restores BBB integrity, reduces cerebral Aβ load, reduces cerebral TJ disruption, halts the pathogenic neoangiogenesis and reverses cerebral hypervascularity. Perhaps most notably, treatment with Axitinib profoundly reduces cognitive impairment. Overall, we conclude that AD can be effectively treated in a preclinical model using an anti-cancer drug that inhibits aberrant neoangiogenic expansion.

Implications of all the available evidence

Our study provides intriguing parallels between AD and otherwise disparate diseases where aberrant neoangiogenesis occurs, such as in the wet form of AMD and in various solid tumours. Repurposing previously approved anti-angiogenic drugs provides a clear path for entry into clinical trials for treating AD. The target for anti-angiogenics in AD is the disrupted neurovascular unit, which is readily accessible by orally administered drugs that enter the bloodstream. Thus, there is no requirement for these therapeutics to actively cross the intact BBB to enter the central nervous system. Finally, this study validates future clinical exploration of other approaches for halting and reversing aberrant cerebrovascular neoangiogenesis to treat AD.

cognition and behaviour in an estimated 50 million people worldwide https://www.who.int/news-room/fact-sheets/detail/dementia [1]. Therapeutics based on the current dogma of AD pathogenesis have been mostly unsuccessful. Notably, in recent years, 65% of clinical trials for AD have involved therapeutics directed against amyloid beta (Aβ) as a pharmacological target [2–4]. Unfortunately, these trials have generally failed to reach their respective therapeutic endpoints and are not curative. As a corollary, these trials have also failed to validate Aβ as a therapeutic target. This suggests that there exists a translational gap between pre-clinical and clinical trials of AD. [2,5]. Furthermore, currently approved treatments for AD are considered "symptomatic" agents that seek to improve cognitive and behavioural symptoms but do not alter the underlying course of AD [2,5]. Clearly, new approaches and therapeutic agents are urgently needed in the AD therapeutic pipeline [2,3,6]. More recently, as a result of the generally bleak clinical trial results, therapeutic pipelines have trended away from targeting Aβ directly and towards other disease targets [1–3].

Growing evidence supports the concept that, in addition to neurons themselves, the neurovascular unit is altered in AD [7–13] and that the disease may be mediated by vascular pathogenesis [7,14,15]. Vascular risk factors and neurovascular dysfunction associated with hypotension, hypertension, cholesterol levels, type II diabetes mellitus, smoking, oxidative stress and iron overload, including the risk factor Apolipoprotein E epsilon 4 allele (APOEε4), are increasingly found to play integral roles in the pathogenesis of stroke and AD [11,15,16]. Notably, cerebrovascular amyloid angiopathy (CAA) is present in the majority of AD cases [16] and is characterized by the presence of Aβ in the pial and intracerebral small arteries and capillaries [17,18], and is associated with microaneurysms and dementia [19]. Additionally, Aβ deposition also causes smooth muscle degeneration and increased vessel stiffness [8], which further degrades the integrity of the vessels.

Vascular dysfunction is gaining acceptance as a crucial pathological hallmark underlying AD pathogenesis [7,11,14,15,25,26] however, the mechanism underpinning these observations has only begun to be illuminated. Studies in AD mouse models [22,23] and in postmortem studies on human brain tissues [24] indicate that pathogenic cerebrovascular neoangiogenesis and blood-brain barrier (BBB) tight junction disruption and vessel leakage appear to occur as a compensatory response to impaired CBF [20,21,28]. These observations have led to an alternative hypothesis where cerebrovascular neoangiogenesis caused by amyloidogenesis and underlying CBF impairment leads to defective neuro-vasculature, thereby disrupting the BBB and further impairing CBF, thus compromising the clearance of Aβ [14,26]. Thus as a result of its vasculotropic activity, Aβ promotes vascular pathology and hence a vicious cycle of abnormal cerebrovascular neoangiogenesis may be established in the disease [7,10,12,14,20,27-29].

Validation of emerging therapeutics for treating AD requires proof of concept trials in preclinical models. In one commonly employed preclinical AD model, the Tg2576 transgenic mouse over-expresses a mutant form of the human amyloid precursor protein (APP isoform 695) with the human Swedish mutation (KM670/671NL), resulting in elevated levels of Aβ in the brain. This model has been well characterized for the development of AD-associated plaques at 9-months of age and cognitive decline starting at 6-months of age and progressing until the animal's death [35]. Our previous work documented that vascular pathology and BBB disruption is observed in the Tg2576 model at 4-months of age and most notably, it preceded the formation of amyloid plaques [7]. Furthermore, we have shown that cerebral hypervascularity and neoangiogenesis give rise to aberrant and leaky cerebral blood vessel formation in the Tg2576 AD model and these features can also be observed in AD patients. Finally, BBB leakage first noted in this model [7,10,12,14] has recently been proposed as an early biomarker in patients with AD [38,39].

These observations prompted us to test the hypothesis that elevated neoangiogenesis underpins AD pathogenesis and that anti-cancer drugs that inhibit neoangiogenesis, can reverse AD-associated pathology. Therefore, here we examine whether the anti-cancer drug, Axitinib (Inlyta; Pfizer), halts and reverses cerebral vessel growth and thereby resolves AD pathology in the Tg2576 mouse model. Axitinib is a tyrosine kinase (TK) inhibitor of vascular endothelial growth factor receptors (VEGFR) [30–33]. It is a second-generation TK inhibitor that has 50–450 times more potency than first-generation inhibitors like Sunitinib (Sutent; Pfizer), that is a less-specific multi-targeted TK inhibitor. Axitinib, that has been shown to block angiogenesis and subsequent tumour growth and metastasis, is

approved for use in treating renal cell cancer in the USA, Canada, Europe, the UK, and Australia, [30,34].

The objective of the current study is to establish the effect of Axitinib, a second-generation anti-angiogenic cancer drug, on memory and cognition in Tg2576 AD model mice and to demonstrate whether neoangiogenesis, BBB leakiness, and Aβ deposition can also be resolved by this new mode of therapeutic intervention.

2. Methods

2.1. Mice

The Tg2576 AD model mouse expresses the Swedish mutant of the amyloid precursor protein (K670N/M671L) under control of the hamster prion protein promoter [35,40]. These mice were provided by Dr. Karen Hsiao Ashe (University of Minnesota) [35] and Tg2576 and wild-type (WT) littermates were maintained at the University of British Columbia. Mice were maintained on mixed C57Bl6/SJL background by mating heterozygous Tg2576 males to C57Bl6/SJL F1 females. WT littermates were used as controls. Aged Tg2576 and WT mice of both sexes were used at 10 months of age. Mice were individually genotyped by PCR [40]. Briefly, two parallel PCR reactions were performed to distinguish heterozygotes from WT. The PrP-APP fusion DNA (corresponding to the heterozygote) was amplified using primers 1502 (hamster PrP promoter, 5'-GTGGATAACCCCTCCCCCAGCCTAGACCA-3') and 1503 (human APP, 5'-CTGACCACTCGAC CAGGTTCTGGGT-3'). The primer combination 1502 and 1501 (mouse PrP, 5'-AAGCGGCCAAAGCCTGGAGGGTGGAACA-3') was used as a positive control for the reaction. The numbers of mice used in the respective experiments are noted in the figure legends. Mice were fed standard lab chow and water *ad libitum* and kept under a 12 h light/dark cycle. All protocols and procedures involving the care and use of animals were reviewed and approved by the UBC Animal Care Committee, which operates under the guidance of the Canadian Council for Animal Care.

2.2. Antibodies and chemicals

Antibodies used for immunoblots, immunofluorescence and immunoprecipitation (concentrations were used according to company datasheets unless indicated otherwise): Goat anti-human endoglin / CD105 polyclonal antibody (RRID: AB_354598 R&D systems; AF1097 https://resources.rndsystems.com/pdfs/datasheets/af1097.pdf?v=20210622&_ga=2.123831427.868075561.1624393141-1326343303.1619741954), anti-β-Amyloid, 1-16 clone 6E-10 (BioLegend; 39320 https://www.biolegend.com/en-us/global-elements/pdf-popup/purified-anti-beta-amyloid-1-16-antibody-11228?filename=Purified%20anti-beta-Amyloid%201-16%20%20Antibody.pdf&pdfgen=true), Polyclonal Antibody Z0-1 (RRID: AB_2533938 ThermoFisher Scientific; cat. # 61-7300 https://www.thermofisher.com/order/genome-database/dataSheetPdf?producttype=antibody&productsubtype=antibody_primary&productId=61-7300&version=156), Recombinant anti-GAPDH antibody [EPR16891] (RRID: AB_2630358 abcam; ab181602), anti-Actin (C-11) antibody (RRID: AB_630835 Santa Cruz Biotechnology; sc1615 https://search.cosmobio.co.jp/cosmo_search_p/search_gate2/docs/SCB_/SC1615.20070227.pdf), rabbit anti-human occludin polyclonal antibody (RRID: AB_881773 abcam; ab31721), anti-CD31 antibody (RRID: AB_726362 abcam; ab28364), anti-mouse serum albumin antibody (RRID: AB_777886 abcam; ab19194), anti-amyloid (1-16) antibody 6E10 (Biolegend; cat. # 803002 https://www.biolegend.com/en-us/global-elements/pdf-popup/purified-anti-beta-amyloid-1-16-antibody-11228?filename=Purified%20anti-beta-Amyloid%201-16%20%20Antibody.pdf&pdfgen=true), beta Amyloid 1-42 anti-amyloid antibody (RRID: AB_867645 abcam; ab39377). The antibody 6E-10, although generally specific for human Aβ, is able to detect mouse Aβ under non-reducing conditions [41]. All antibodies were commercially sourced and their specificity was validated by the suppliers.

Chemicals used: 10% Nonidet P-40 (NP-40), detergent. 10% solution in water (RRID: abcam; ab142227), 100 X Halt protease and phosphatase inhibitor cocktail (RRID: ThermoFisher Scientific; cat. # 78440).

2.3. Immunoblotting analysis

For immunoblot analysis, the fractional homogenate samples were prepared using reducing sample buffer (100 mM Tris-Cl (pH 6.8), 4% (w/v) SDS, 0.2% (w/v) bromophenol blue, 20% (v/v) glycerol and 200 mM 1-4, dithiothreitol, DTT). Proteins in homogenates were separated using polyacrylamide gel electrophoresis and were identified using primary antibodies after transfer of proteins to nitrocellulose membranes using standard methods. The immunoblots were imaged using the Odyssey infrared image system (LICOR Inc.) and relative levels of immunoreactivity were analyzed using Image Studio ^{TM} Lite software (LICOR Inc.).

2.4. Pharmacological treatments

Axitinib (LC laboratories, MA) was administered to the Tg2576 mice and their WT littermates. Control groups containing both Tg2576 and WT animals were given the drug delivery vehicle (PBS +DMSO) alone. Axitinib at a dose of 10 mg/kg (dissolved in 100% DMSO at 40 mg/ml and subsequently diluted to the desired concentration in PBS) or the drug delivery vehicle alone administered to the mice via oral gavage. Mice were treated three times a week for a duration of one month before testing the animals for cognitive performance. Cognitive testing entailed evaluation of different aspects of memory and learning using a battery of tests including the open field test, Y-maze, fear conditioning and radial arm water maze, before euthanizing the mice prior to histological and biochemical analysis of brain tissue.

2.5. Open field test

A plexiglass chamber measuring 50 x 50 x 38 cm with dark-coloured walls and a light source focused in the centre was used. Animals across all groups were placed one at a time in the arena. The floor of the chamber was demarcated into central and peripheral regions. The field was also calibrated using the computer software, so the camera could create physical distance data from pixel-based information. The system was connected to a black and white analog tracking camera with an RTV24 Digitizer that was placed overhead of the open field. The path travelled and time spent in the different regions of the field were tracked and recorded for a total of 5 min using the computer tracking system (ANY-maze, Stoelting). The test exploits the innate behaviour of 'thigmotaxis' where the mice tend to stay towards the shaded edges of an open field and keep away from the brighter centre. This implies that mice that have intact cognition and awareness of the potential danger in the open field environment will spend less time in the centre of the field. This test assesses an animal's anxiety, locomotion and exploration of a novel environment [36,37].

2.6. Spontaneous alternation test (Y-maze)

The test for novelty exploration using spatial and working memory was conducted using a symmetrical Y-maze with a grey steel bottom plate and grey Perspex® walls (Stoelting Co, Wood Dale, IL) [36,37]. Each arm of the Y-maze measured 35 cm by 5 cm and 10 cm high and the wall at the end of each arm was identified by a different colour: white, blue or red. The spatial acquisition phase comprised a one-day trial with the mice tracked while moving freely through the three arms of the Y maze during an 8 min session. The movements

were tracked by a computer tracking system (ANY-maze, Stoelting). The performance was gauged by the percentage of alternations that was calculated as the total number of alternations × 100/(total number of arm entries − 2). Alternation was defined as successive entries into the three arms on overlapping triplet sets. A high percentage of alternation was indicative of sustained cognition, as the animals must remember which arm was entered last to avoid re-entering it.

2.7. Contextual fear conditioning test

The apparatus consisted of a transparent chamber inside an enclosure with an opening in the ceiling to allow video recordings. The chamber consisted of a steel grid floor connected to a shock generator scrambler. The test encompassed two sessions: conditioning and a context test. On the conditioning day, the mice were individually placed in the chamber and allowed to explore freely for 5 min during which, at the 180th second, they received a foot shock of 0.50−0.80 mA for 3 s through the bars of the floor. Twenty-four hours after conditioning, the mice were individually placed back in the chamber for 4 min, this time with no noxious stimuli. The mice were monitored for movement and freezing behaviour was recorded using computer software (Limelight, ActiMetrics, Wilmette, IL, USA). Exclusion criteria were set for freezing events of less than 2 s. This test was used to determine associative working memory. We explored the animal's ability to associate an environment with a noxious event that it experienced there. When the animal is returned to the same environment, it generally will demonstrate a freezing response if it remembers and associates that environment with the shock. Freezing is a species-specific response to fear, which is defined as "the absence of movement except for respiration". This may last for seconds to minutes depending on the strength of the aversive stimulus and whether the subject is able to recall the shock [36,37].

2.8. Radial arm water maze (RAWM)

The RAWM contains eight swim paths (arms) extending out of an open central area, with an escape platform located at the end of any of four alternate arms called the 'goal arms' [36,37]. The start position and the goal arms were fixed throughout the duration of the study. The mice were individually placed at the 'start position' of the maze and given 60 s to locate one of the 4 escape platforms. With each trial, the platform that was used to escape was removed and not placed back into the maze until the end of that test day. The test was repeated until only one platform was left. Once the animal found the last platform it marked the end of the test for that day. In between each trial, the animal was removed and placed back in its heated home cage for 90 s to avoid hypothermia. These trials were conducted daily for a total of 5 days. The latency to reach the platform for each trial and the arm entries were recorded manually. Performance of memory and learning was gauged each day based on the average time taken to find the escape platforms and the total number of errors, *i.e.* reference memory errors + working memory errors. A reference memory error is defined as the entry into an arm that never had an escape platform and a working memory error is defined as the subsequent entry into an arm where the platform had been removed in the previous trial.

2.9. Tissue preparation

After the behaviour studies, the animals were terminally anesthetized with ketamine/xylazine (100 mg/kg; 10 mg/kg) and perfused with PBS for 5 min at a 5 ml/minute flow rate. Brains were removed, one hemisphere was fixed with 4% paraformaldehyde (PFA) for histology and stored at 4 °C and the other hemisphere was flash-frozen for biochemical studies and stored at -80 °C. The PFA fixed hemispheres were embedded in a 4% agarose block and microtome sectioned to be used for immunofluorescence analysis, whereas the flash-frozen mouse brain hemispheres were homogenized mechanically using a douncer. The cytosolic fraction was used to detect soluble proteins. The pellet left behind after the initial solubilization and centrifugation was resuspended in 2% sodium dodecyl sulphate (SDS) solution in dH_2O. The supernatant from this treatment contained the membrane-bound proteins. The portion of the pellet that was not dissolved in 2% SDS contained the plaque-associated Aβ that was solubilized by 70% sulfuric acid treatment, lyophilized, and resuspended in 1X PBS solution. Halt protease and phosphatase inhibitor cocktail (1X; ThermoFisher Scientific; 78440) was added to prevent protein degradation.

2.10. Immunofluorescence and confocal microscopic imaging

The brain hemispheres fixed with 4% PFA overnight were transferred into PBS + 0.01% sodium azide and stored at 4 °C. The fixed hemispheres were subsequently embedded in 4% agarose and sectioned at a thickness of 50 μm. Mouse hippocampus (CA1 and DG) and cortex (entorhinal and prefrontal cortex), regions involved in learning and memory that are affected in AD, were examined microscopically after immunohistochemical staining. Brain sections were treated with blocking buffer (3% skimmed milk in PBS; 0.1% Tween-20) for 1 hour at room temperature followed by overnight incubation at 4 °C with primary antibodies against the various proteins of interest: CD105 (R&D Systems; AF1097), Aβ (BioLegend; 39320) and tight junction protein Occludin (abcam; ab31721), CD-31 (abcam; ab28364) and albumin (abcam; ab19194). For colocalization experiments, multiple antibodies were simultaneously used on the sections. Incubation with fluorophore-conjugated secondary antibodies was performed at room temperature for 1 h. Nuclear counterstaining was performed using diamidino-2-phenylindole (DAPI), a blue fluorescent probe that fluoresces brightly upon selectively binding to the minor groove of double-stranded DNA. Sections were then washed using PBS containing 0.1% Tween-20 before the addition of Fluoromount-G™ Mounting Medium (Catalog number: 00-4958-02, Thermo Fisher) and protective coverslips. Slides were allowed to air-dry overnight in the dark.

Image acquisition was performed using an Olympus FV-10i confocal microscope with a high-resolution Olympus 60 X/1.4 oil-immersion objective. For 3-D image data acquisition, the excitation beam was first focused at the maximum signal intensity focal position within the brain tissue sample and the appropriate exposure times were selected to avoid pixel saturation. A series of 2-D images (*Z* stack) were taken at a step size of 1 μm. The beginning and end of the 3-D stack acquisition were set based on the signal level degradation. Volocity software (PerkinElmer; http://cellularimaging.perkinelmer.com/pdfs/manuals/VolocityUserGuide.pdf) was used to process the series of images for the generation of a 3-D reconstruction of the tissue.

Volume estimation was performed on the 3-D image data sets recorded from the cortical or hippocampal region of brain sections. In this procedure, a filter (either Gaussian or kernel size of 3 × 3) was used to remove the noise associated with the images. To define the boundary between the objects (for instance, blood capillaries or amyloid) and the background, the lower threshold level in the histogram was set to exclude all possible background voxel values. The sum of all the voxels above this threshold level was determined to be the volume. The total fluorescence volume (TFV) was detected in the field of interest and was integrated above the background by the software. The ratio of the TFV and the total volume of the field was used as a numerical representation of the expression of the protein of interest in a unit volume of the voxel. Colocalization of proteins was established by selecting the background as an area of interest (http://cellularimaging.perkinelmer.com/pdfs/manuals/VolocityUserGuide.pdf). Illumination and background correction were performed by the

software for saturated voxels. The thresholds for different channels/target proteins were set using this region of interest. Clicking a point outside the region of interest yielded the scatter plot for the entire image (http://cellularimaging.perkinelmer.com/pdfs/manuals/VolocityUserGuide.pdf). The colour in the scatterplot represents the number of pixels that are plotted in that region. The intensity of one channel is shown on the x-axis and the intensity of the second channel is shown on the y-axis. Thresholded Pearson's Correlation Coefficient (PCC) was calculated using the Volocity software (http://cellularimaging.perkinelmer.com/pdfs/manuals/VolocityUserGuide.pdf). Statistical significance was calculated using an online free statistics calculator (https://www.danielsoper.com/statcalc). The closer the value of PCC is to 1, the stronger the statistical correlation is between the two targets.

2.11. Semi-quantitative analysis of tight junction (TJ) morphology

Brain sections were examined by immunofluorescence for co-localization of CD-31 and occludin proteins. In the hippocampus and cortex, individual vessels stained with anti-CD31 were scored as either normal ("1") or abnormal ("0") for occludin expression. Normal occludin expression was defined by observation of strong, continuous, intense linear staining. In contrast, abnormal occludin expression was judged as weak, punctate and/or discontinuous staining. To minimize the recording of incomplete or undulating vessels as abnormal due to observed "gaps" in occludin staining, evidence of vessel continuity was sought in the images with the help of CD31 staining. The percentage of tight junction disruption in a given region of the brain was defined as the percentage of blood vessels that displayed abnormal TJ morphology. The image acquisition and analysis were performed as described above.

2.12. Blood-brain barrier (BBB) permeability assay

Evans Blue is a dye that has a high affinity for serum albumin [10]. An intact BBB is impermeable to serum albumin and thus the injected Evans Blue remains bound to the serum albumin and does not stain the neuronal tissue. When the BBB has been compromised, albumin-bound Evans Blue dye enters the CNS and stains it blue, allowing visual qualitative confirmation in addition to the quantitative immunofluorescence assay Drug- and vehicle-treated mice (n = 3) were weighed and injected intraperitoneally (i.p.) with Evans Blue dye (Sigma Aldrich, #E2129), 50 μg (in 100 μl PBS) per gram weight of the mouse [10,42]. Three hours after injection, the mice were terminally anesthetized with ketamine (100 mg/kg i.p.; Narketan, Vetoquinol) and xylazine (10 mg/kg i.p.; Rompun, Bayer) and transcardially perfused with PBS for 5 min at a 5 ml/minute flow rate [10]. After removing the cerebellum and olfactory bulbs, the brains were weighed. The Evans blue dye was extracted as follows: one mL of 50% trichloroacetic acid was added to the brain and the samples were Dounce homogenized by pulling the plunger up and down 10 times. The homogenates were centrifuged at 19000 g (approx. 13,000 rpm) for 10 min and the supernatant diluted 1:4 with 100% ethanol. The optical density of the supernatant was read with an ELISA plate reader (Spectra Max 190; Molecular Devices, Sunnyvale, CA) at 620 nm [42]. The readings were divided by the weight of the brain and the data were statistically analyzed with unpaired t-tests.

2.13. Statistical analysis

Data are presented as the mean ± standard deviation. Statistical analyses were performed with the help of GraphPad Prism software using unpaired Student's t-test when comparing two groups and a 2-way ANOVA test for multiple comparisons with a Bonferroni's test to correct for the multiple comparisons. The Thresholded Pearson correlation co- efficients were calculated with the help of the online free Statistics Calculator, ver. 4.0 (https://www.danielsoper.com/statcalc). The sample size for each experiment is indicated in the figure legend. Bar graphs were generated using GraphPad Prism software (GraphPad Prism Software, San Diego, CA). Protein levels involved with angiogenesis in Tg2576 mice were calculated by normalizing the mean pixel density with values from the WT (B6/SJL) mice.

2.14. Statement of Ethics

Animal-Use Ethics: Animal experimentation was overseen and approved by the Animal Care Committee at the University of British Columbia, which operates under the guidelines of the Canadian Council for Animal Care.

Funding: The funding sources had no role in the study design, data collection, analysis or interpretation of data, or in the writing of the paper.

3. Results

3.1. PK and stability trial

The no-observed-adverse-effect-levels (NOAELs) for Axitinib in mice were set at <10 mg/kg/day for 26 weeks of once-daily oral gavage administration (https://hpr-rps.hres.ca/reg-content/summary-basis-decision-detailOne.php?lang=en&linkID=SBD00071). A study in humans found that the half-life of Axitinib ranges from 2.5 to 6.1 h and that plasma half-life was not changed appreciably in fed and fasted states (https://pdf.hres.ca/dpd_pm/00054598.PDF)[47]. Furthermore, PK studies showed that plasma levels of Axitinib reached a steady-state within 15 days, with no unexpected accumulation [43]. Active anti-angiogenic doses in mice have been observed between 1 and 10 mg/kg/day [44]. We undertook a PK study to determine the initial plasma concentrations in mice that were gavaged with 10 mg/kg of the drug. Six different time points were chosen for initial PK studies (2, 4, 6, 8, 10, 12 h) and for steady-state at 24 h and 48 h. One hundred μl of blood and whole-brain tissues were taken from each mouse for analysis of the absorption, distribution, metabolism and excretion of the drug at the given time points. We subcontracted MRM Proteomics (http://www.mrmproteomics.com) to analyze the plasma samples for the presence of Axitinib, according to published pharmacokinetic data [44]. The liquid chromatography-mass spectrometry (LC-MS) system, assay development and Axitinib quantitation are described in the supplementary file. **Fig. 1** depicts the concentration of Axitinib in the brain and plasma of mice at different time points. The bioavailability of the drug was calculated from the area under the curve. This PK study helped determine the schedule for treating the hypervascularity observed in AD. We initially treated the Tg2576 mice and WT littermates with Axitinib at concentrations of 10 mg/kg/day as it is the highest concentration reported in the literature to have no adverse side effects. The reported schedule of 10 mg/kg/day was administered as an acute treatment for cancer, hence we decided to initially schedule a treatment of 10 mg/kg 3 times a week for 1 month.

3.2. Axitinib treatment restores the behaviour of Tg2576 AD mice

The ultimate goal of treatment for AD patients is to restore normal cognition and behaviour. Thus, in the pre-clinical model studied here, we used several different behavioural tests to assess the cognitive status of Axitinib-treated mice. Both male and female transgenic Tg2576 AD mice and their WT B6/SJL littermates were treated with either Axitinib or vehicle alone (PBS+DMSO) 3X/week for one month, starting at 10 months of age. No differences were observed between male and female mice in the behavioural testing or in their response to the treatments, so the data from males and females were combined. Data from 3 separate mouse trials were pooled for statistical

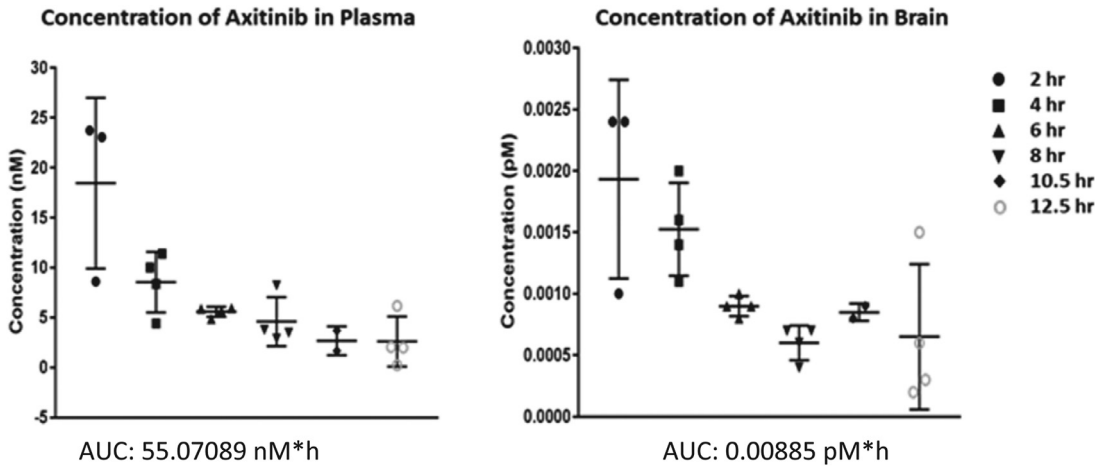

Fig. 1. Concentration of Axitinib measured in mouse plasma and brain. Pharmacokinetic analysis of Axitinib at 10 mg/kg/mouse at different time points to demonstrate the bioavailability of the chosen drug dosage. The concentration of Axitinib in the samples was calculated from the linear-regression calibration curve with internal standard calibration. AUC= area under the curve. The curve represents the metabolism of the drug over time and the AUC represents the total drug exposure over time.

analysis (WT vehicle-treated and WT Axitinib-treated, n = 15 each; Tg2576 vehicle-treated and Tg2576 Axitinib-treated, n = 20 each)**.**

The Open Field Test: The Open Field Test was used to assess the natural aversion (awareness) shown by mice in a novel brightly lit open arena, as well as general locomotor activity levels. It was observed that the WT mice (pre-treatment and treated) spent a majority of the time confined to the peripheral region of the field and rarely explored the centre of the open field, which is inherent to their nature **(**Fig. 2**a,b)**. On the other hand, the pre-treatment and the vehicle-treated Tg2576 AD mice explored the entire field indiscriminately, with more distance travelled compared to all the other groups and significantly more time in the centre of the field compared to their respective WT littermates **(**Fig. 2**a,b)**. However, after treatment with Axitinib, the Tg2576 mice behaved more like WT mice, exploring the field to a lesser extent, preferring to move along the wall instead of into the open central area, and spent significantly less time in the centre as compared to the pre-treatment and vehicle-treated Tg2576 mice **(**Fig. 2**a,b)**.

The Y-maze test: Spatial and working memory assessment was performed using a spontaneous alternation test (Y-maze). Pre-treatment and vehicle-treated WT mice showed an alternation of 67 ± 5.5% (mean± standard deviation) and 70 ± 13.8% respectively, with no significant change observed when WT mice were treated with Axitinib **(**Fig. 2**c)**. In contrast, pre-treatment and vehicle-treated Tg2576 AD mice showed poor performance on the test compared to their respective WT littermates, with a significantly lower percentage of alternation 52.8 ± 4.7% and 41.2 ± 8.3% respectively **(**Fig. 2**c)**. Axitinib-treated Tg2576 mice showed significantly more alteration than pre-treatment and vehicle-treated Tg2576 mice, a performance that was indistinguishable from WT mice.

Contextual Fear Conditioning test: In contextual fear conditioning, associative memory is assessed where normal mice are expected to "freeze" (remain stationary) after being placed in an environment where they had previously received an electric shock. Pre-treatment, vehicle-treated and Axitinib-treated WT mice exhibited good associative memory scores by showing freezing percentages of 15.9 ± 3.2%, 18.51 ± 9.1% and 17.74 ± 14.4%, respectively **(**Fig. 2**d)**. The vehicle-treated Tg2576 AD mice showed significantly lower freezing scores (2.3 ± 1.5%), while the scores of Axitinib-treated Tg2576 animals were similar to those of WT control animals (14.4 ± 7.3%).

Radial Arm Water Maze: Evaluation of reference memory (long-term) and working memory (short-term) was performed by testing mice with the Radial Arm Water Maze (RAWM). Fig. 2**e** shows the total latency time whereas Fig. 2**f** shows the number of errors made by the mice when locating the submerged escape platform. A comparison of the number of errors and the latency time was made between the first test day and the fifth test day within each group. Significant differences in the performance on the first test day versus the fifth test day were observed in the pre-treatment WT mice, vehicle-treated WT mice and the Axitinib-treated WT mice. No significant difference was observed in the pre-treatment Tg2576 mice and the vehicle-treated Tg2576 mice on the first day compared to the fifth day. Interestingly, Axitinib-treated Tg2576 mice showed a significant difference in the latency time and the number of errors when performance was compared between the first test day and the fifth test day. The latency time and the number of errors made on the fifth test day were compared between the different groups. A significant decrease in the latency time and the number of errors between pre-treatment WT mice and pre-treatment Tg2576 mice, as well as between vehicle-treated WT and vehicle-treated Tg2576 mice was observed. A significant decrease in the latency time and the number of errors was also observed between the pre-treatment and Axitinib-treated Tg2576 mice, as well as between the vehicle-treated and Axitinib-treated Tg2576 mice. No significant difference was observed in the latency time and the number of errors between the fifth-day performance of the Axitinib-treated WT and the Axitinib-treated Tg2576 mice. Thus, the Axitinib-treated Tg2576 mice showed cognitive learning (reference memory and working memory) that was indistinguishable from WT animals.

3.3. Axitinib treatment reduces cerebrovascular pathology

To assess the effect of the drug on AD pathology, the brains of treated mice were analyzed by semi-quantitative immunoblotting to look for expression of the neoangiogenic marker CD105, Aβ, amyloid precursor protein (APP) and the tight junction protein, ZO1. Treatment of the Tg2576 mice with Axitinib for one month resulted in a significant decrease in the expression of the angiogenic marker CD105 compared to the vehicle-treated Tg2576 mice (Fig. 3**a**). Interestingly, in Axitinib-treated Tg2576 animals, there was also a significant decrease in Aβ expression by more than one-half in comparison to the vehicle-treated Tg2576 mice (Fig. 3**c**). In contrast, expression of the tight junction protein ZO-1 was increased in the Axitinib-treated Tg2576 mice when compared to the vehicle-treated Tg2576 mice (Fig. 3**b**).

Immunofluorescence microscopic analysis of these proteins in both the cortex and hippocampus of the mouse brains confirmed the immunoblotting data. Fig. 4 shows representative immunofluorescence micrographs of the cortex whereas the histograms are

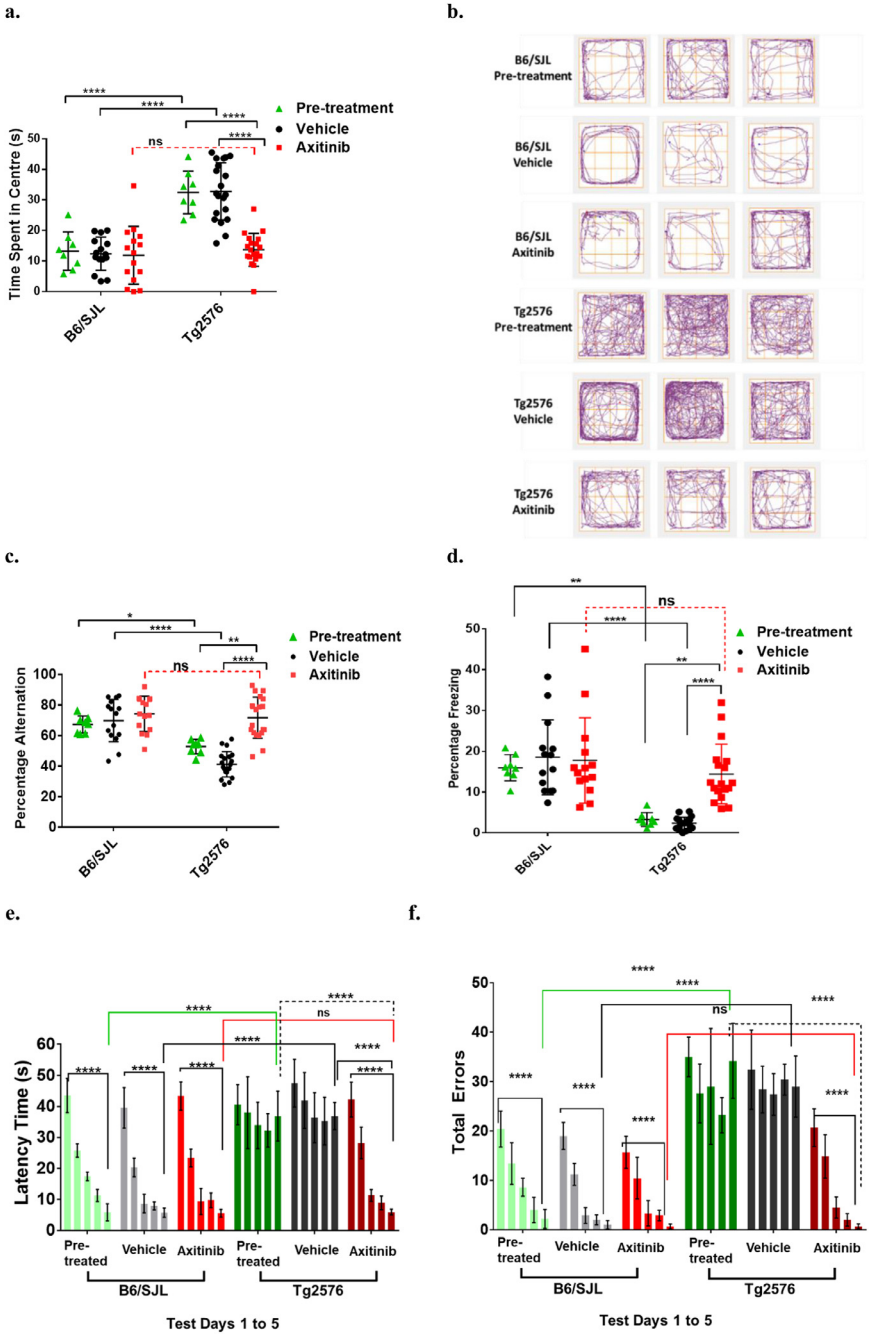

Fig. 2. Effect of treatment with the anti-angiogenic drug, Axitinib, on cognitive impairment in aged Tg2576 mice. Pre-treatment 10-month old mice and post-treatment 11-month old mice were assessed for their cognitive status, using tests designed for the analysis of different aspects of memory. The data were pooled from 3 different trials and are represented as the mean± standard deviation. Statistical analysis was performed using a 2-way ANOVA with correction for multiple comparisons using the Bonferroni's test (* $p<0.03$; ** $p<0.002$; *** $p<0.0002$; **** $p<0.0001$). **a) Open Field Test.** WT mice spent less time in the center of the field, with no significant difference observed between pre-treated mice and those treated with Axitinib. Vehicle-treated Tg2576 AD mice spent significantly more time exploring the center of the field than Axitinib-treated Tg2576 mice or WT mice. A significant difference was observed between the pre-treatment WT and Tg2576 AD animals. A significant difference was also observed between pre-treatment Tg2576 and Axitinib-treated Tg2576 mice. No significant difference was observed when the WT mice and Axitinib-treated Tg2576 mice were compared. **b) Representative track plots from the open field test.** Cognitively aware WT and Axitinib-treated Tg2576 mice spent less time exploring the open center of the test arena and more time exploring the edges than cognitively impaired pre-treatment and vehicle-treated Tg2576 mice. Each box in the figure represents the track from a different mouse. **c) Spontaneous alternation (Y-maze) Test.** A high percentage of alternation was observed in the pre-treatment WT mice, with no significant difference observed after treatment with the vehicle alone or after treatment with Axitinib. Pre-treatment and vehicle-treated Tg2576 mice exhibited poor performance on the test, with a significantly lower percentage of alternation compared to the pre-treatment and vehicle-treated WT mice, respectively. Axitinib-treated Tg2576 mice showed a significantly higher rate of alternation compared to the pre-treatment and vehicle-treated Tg2576 mice. No significant difference was observed between the WT mice and the Axitinib-treated Tg2576 mice. **d) Contextual Fear conditioning Test.** Pre-treatment, vehicle-treated and Axitinib-treated WT mice exhibited good associative memory by showing high freezing percentages. The pre-treatment and vehicle-treated Tg2576 mice displayed a significantly lower freezing percentage compared to the pre-treatment and vehicle-treated WT mice, respectively. Axitinib-treated Tg2576 animals performed similarly to the WT mice. Axitinib-treated Tg2576 mice showed significantly higher performance compared to pre-treatment and vehicle-treated Tg2576 mice. **e-f) Radial arm water maze.** Both latency time (the time it took for the mice to locate the escape platforms) (**e**) and the number of working and reference memory errors made by the mice when locating the escape platforms) (**f**) were measured. Pre-treatment, vehicle- and Axitinib-treated WT mice showed a significant decrease in the latency time and decreased the number of errors made when comparing results from test day 1 and test day 5. A similar improvement throughout the trial was observed in the Axitinib-treated Tg2576 mice. No significant differences between test day 1 and test day 5 were observed in the pre-treatment and the vehicle-treated Tg2576 mice.

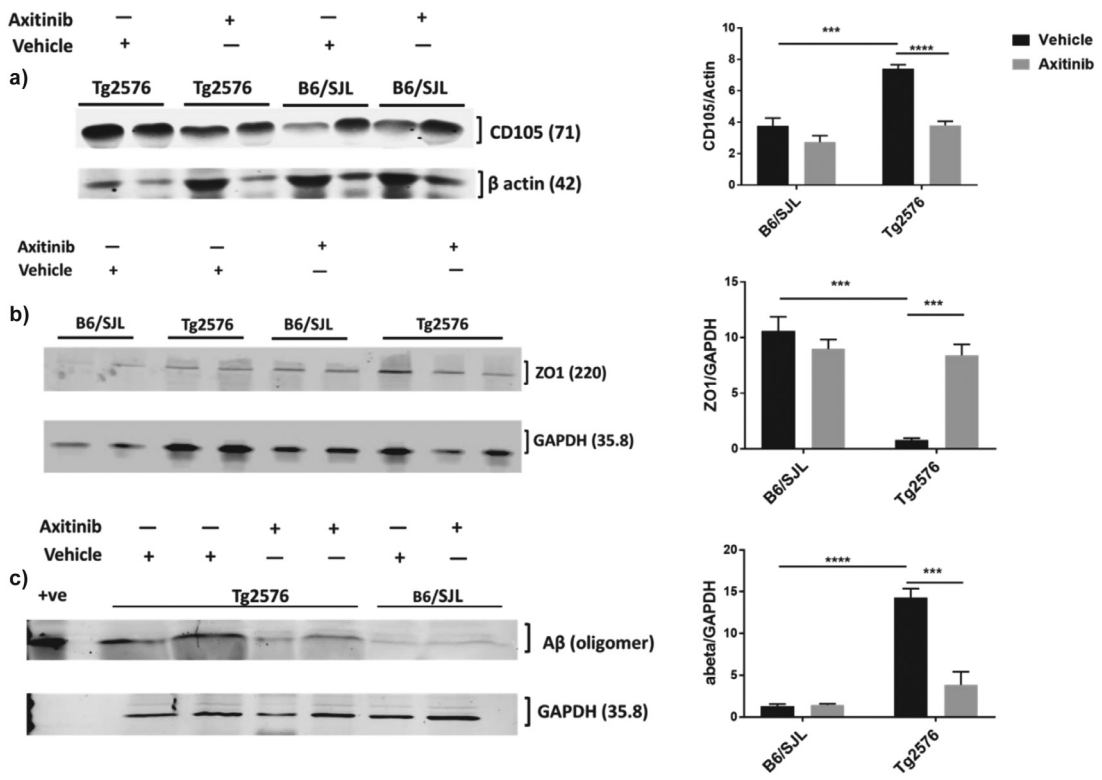

Fig. 3. Expression of Aβ, the angiogenic marker CD105 and the tight junction protein, ZO1 in aged WT and Tg2576 mice. Whole-brain homogenates from perfused mice were used for molecular analysis of the different biomarkers by immunoblotting. **a)** Expression of the angiogenesis marker CD105 was significantly higher in the brains of vehicle-treated Tg2576 mice than in the brains of Axitinib-treated Tg2576 or WT animals. **b)** The expression of tight junction protein, ZO1, was significantly lower in the vehicle-treated Tg2576 mice when compared to the WT mice or Axitinib-treated Tg2576 mice. **c)** The presence of Aβ in the Tg2576 mouse brain was much higher in the vehicle-treated than in Axitinib-treated animals, resembling background levels (e.g. those observed in WT brains). Representative immunoblots are shown for mice from different groups. The anti-Aβ antibody used here was initially made against human amyloid but cross-reacts with mouse amyloid under reducing conditions. The data in the histograms are representative of means of individual animals with error bars representing the standard deviation from the mean observed in three separate experiments with WT n= 6 and Tg2576 n= 6 per treatment group. A two-tailed unpaired t-test with was used to calculate significance **(* $p<0.03$; ** $p<0.002$; *** $p<0.0002$; **** $p<0.0001$).**

representative of analyses from the cortex and hippocampus. Aβ staining was significantly more prevalent in the brains of vehicle-treated Tg2576 mice than in the brains of Axitinib-treated Tg2576 animals (Fig. 4**a**). The staining of the mature blood vessel marker, CD31, was similar in all the different groups. However, CD105, the sprouting blood vessel marker, was increased in the vehicle-treated Tg2576 group when compared to the Axitinib-treated Tg2576 or WT mice, indicating a state of hypervascularity in the vehicle-treated Tg2576 animals (Fig. 4**a,b**). Low expression of occludin, a 65 kDa integral plasma-membrane protein used as a marker for tight junctions, was observed in the vehicle-treated Tg2576 when compared to the Axitinib-treated Tg2576 mice and WT (B6/SJL) animals (Fig. 4**b**).

3.4. Axitinib treatment reduces the loss of tight junction structure and BBB integrity in Tg2576 mice

In healthy "normal" animals the physical seal of the BBB is maintained mainly by an intact and continuous arrangement of the tight junction proteins ZO1, claudin and occludin, along with other components of the neurovascular unit. Their alteration can lead to disruption of the tight junctions between the endothelial cells and hence lead to increased permeability of the barrier, resulting in the unhindered movement of toxic blood products into the brain, thus advancing AD pathology. Tight junction protein disruption was analyzed in the brains of Tg2576 mice and their WT littermates. A normal occludin expression pattern, as indicated in Fig. 5**a**, was strong and continuous. It was observed that the WT mice showed a normal expression pattern of tight junction proteins (as indicated with the white arrows in the micrographs) and thus a low percentage of disruption irrespective of Axitinib or vehicle treatment. In the vehicle-treated Tg2576 mice, however, there was a significant increase in the disruption of the tight junction proteins. Tg2576 mice treated with Axitinib showed a lower percentage of the tight junction disruption, similar to that observed in the WT brain sections.

To support the idea that this intact arrangement of the tight junction proteins influenced the permeability of the BBB in the animals, we conducted an Evans Blue assay. Evans Blue dye binds to serum albumin, and a disrupted BBB allows this dye-bound albumin to enter the central nervous system (CNS), as indicated by the presence of the dye in the brain [42]. Fig. 5**b** shows that when Evans Blue dye was injected into mice that have an intact BBB, the dye was unable to cross into and stain the brain, whereas the opposite was true when the BBB is permeable and the brain appears blue. The cerebellum was removed from the brain and then extraction and measurement of Evans Blue was carried out. Fig. 5**c** illustrates the Evans Blue staining measured as absorbance in terms of optical density/unit mass of the brain. Increased absorbance was noted in vehicle-treated Tg2576 mice, indicating substantial Evans Blue uptake in the brain, compared to WT littermates and Axitinib-treated Tg2576 mice. In a separate experiment, brain sections of Tg2576 mice and WT littermates that were treated with Axitinib or vehicle were immunostained to examine the presence of albumin in the brain sections. Representative micrographs of the cortical region of the brain in Fig. 5**d** show the presence of albumin. Minimal amounts of albumin were observed in the WT brains, indicating an intact BBB, whereas substantial staining of albumin was observed in the vehicle-treated Tg2576 mice, implying a disrupted and highly permeable BBB. The brains of the Axitinib-treated

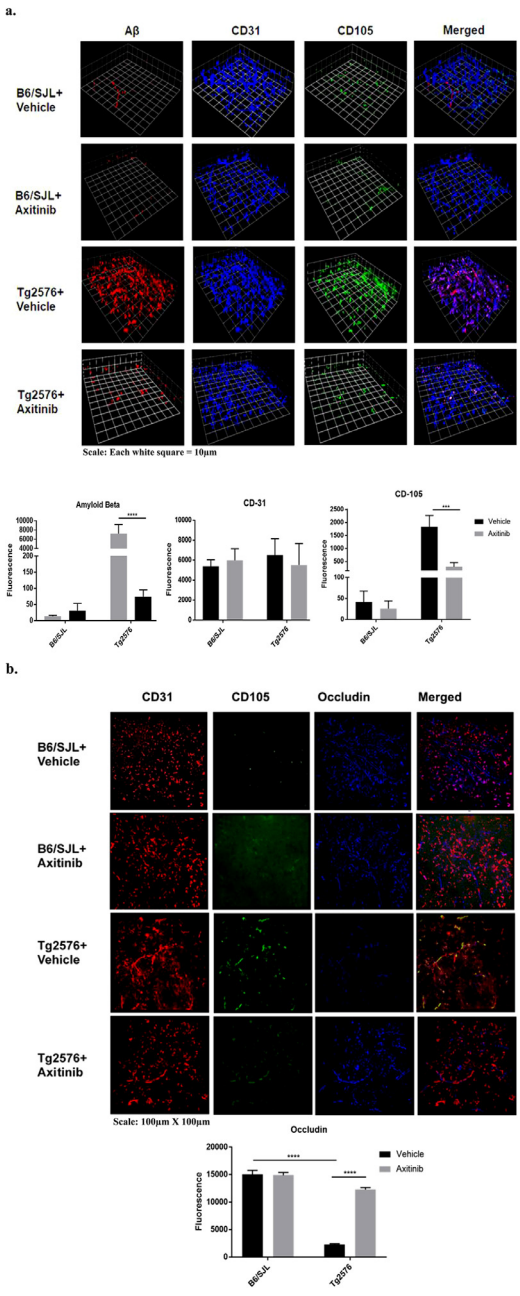

Fig. 4. Multiplexed immunofluorescence analysis of WT and Tg2576 mouse brain sections before and after Axitinib treatment. **a)** Brain sections of mice from different groups were stained for the combination of markers CD105, Aβ and CD31. The micrograph panels are representative of the cortical region of the brains of the mice belonging to the different treatment groups. The white grid is representative of the 3D volume of the field of view. The micrographs show the voxels of the field of view of the imaged sections represented by the grid. The data are represented as the mean± standard deviation. Statistical analysis was performed using unpaired Student's t-test with the same area imaged from n= 4 to 6 animals per treatment group. **(* p<0.03; ** p<0.002; *** p<0.0002; **** p<0.0001).** Aβ (red); CD31 (blue); CD105 (green), and where coincident staining occurs, combinations are as follows: Red + Green = Yellow; Red + Blue = Purple; Blue + Green =Cyan; Blue + Red + Green =White. The dimensions of each micrograph are 100 X100 X 20 μm. (Scale: each white box = 10 μm) **b)** Brain sections of mice from different groups were stained for the combination of markers CD105, CD31 and the tight junction protein, Occludin. The micrograph panels are representative of the cortical region of the brain. CD31 (red); CD105 (green); Occludin (blue) and where coincident staining occurs, combinations are as follows: Red + Green = Yellow; Red + Blue = Purple; Blue + Green =Cyan; Blue + Red + Green =White. Size of micrograph: 100 μm X 100 μm. The data are represented as the mean± standard deviation. Statistical analysis was performed using two-tailed unpaired Student's t-test with the same area imaged from n= 3 animals per treatment group. **(* p<0.03; ** p<0.002; *** p<0.0002; **** p<0.0001). (For interpretation of the references to colour in this figure, the reader is referred to the web version of this article.)**

Tg2576 mice showed less albumin staining, demonstrating a more functional BBB.

Thresholded Pearson's Correlation Coefficients were calculated to assess the correlation between Aβ and CD105 expression and between CD105 and occludin expression in brain sections. A value of "+1", indicates a positive correlation between the two events with an increase in one variable associated with a corresponding increase in the other, whereas "0" would indicate no correlation and "-1" would indicate a negative correlation with an increase in one variable associated with a corresponding decrease in the other. A correlation coefficient of r = +0.62 (one-tail t-test, p = *0.021*) in vehicle-treated Tg2576 mice, which show an overproduction of Aβ, indicated a positive correlation between Aβ and CD105, suggesting a relationship between the presence of excessive amounts of Aβ and an increase in the sprouting pathogenic vessels in the cerebral vasculature. On the other hand, a correlation coefficient of r = -0.73 (one-tail t-test, p = *0.006*) in the vehicle-treated Tg2576 mice indicates that CD105 and occludin expression are negatively correlated.

4. Discussion

Our previous studies identified BBB disruption in both mouse models of AD and in patients with AD [7,10,14] and demonstrated that Aβ driven cerebral vascular neoangiogenesis is the underlying mechanism leading to BBB disruption [7,14]. We subsequently demonstrated that immunization with Aβ results in the resolution of its proangiogenic signal and resolves molecular vascular pathogenesis and cognitive decline in an animal model of AD [12]. Two vascular growth processes have been identified in the formation of new blood vessels from pre-existing vessels. The first, sprouting, is a phenomenon where offshoots grow outward from existing vessels observed in Fig.4 [45] and the second, known as intussusceptive growth, is the process whereby existing vessels divide into two definitive parallel vessels through a multistage [45] process. Normal wound healing angiogenesis is tightly regulated by various growth and tissue factors resulting in minimal changes in microvascular permeability, proteolysis, and inflammation. However, abnormal or pathological neoangiogenesis, has been observed in inflammatory bowel disease and AMD where the vasculature exhibits abnormal architecture, increased permeability, and increased inflammatory and thrombogenic potential. Our data demonstrate that cerebral neoangiogeneis in AD likely occurs through sprouting neoangiogenesis as demonstrated in Fig.4, however, future studies need to be undertaken to determine if intussusceptive neoangiogenesis is also a pathogenic feature in AD [45]. From these studies, we can hypothesize a plausible molecular mechanism underpinning how amyloidogenesis, leading to the activation of pathological neoangiogenesis causes the breakdown of the BBB.

As a consequence of these observations, in the present study, we investigated the effect of a second-generation anticancer small-molecule tyrosine kinase inhibitor, Axitinib, that targets disease-associated vascular neoangiogenesis in a preclinical model of AD. In this report, 10-month old Tg2576 mice and WT littermates (pre-treatment), along with 11-month old Axitinib-treated and vehicle-treated Tg2576 mice and WT littermates, were assessed using multiple paradigms of memory and cognition. WT mice (treated or untreated), and Axitinib-treated Tg2576 mice showed significantly higher cognition compared to the pre-treatment and vehicle-treated Tg2576 mice. Spatial awareness, exploration, associative memory, working memory and reference memory were all increased in Tg2576 mice treated with Axitinib. Axitinib treatment resulted in lower expression of the angiogenic marker CD105, lowered Aβ load, and increased the expression of tight junction proteins ZO1 and occludin, resulting in a more functional BBB in aged Tg2576 mice. Thus, Axitinib can alter cerebral pathology, Aβ load

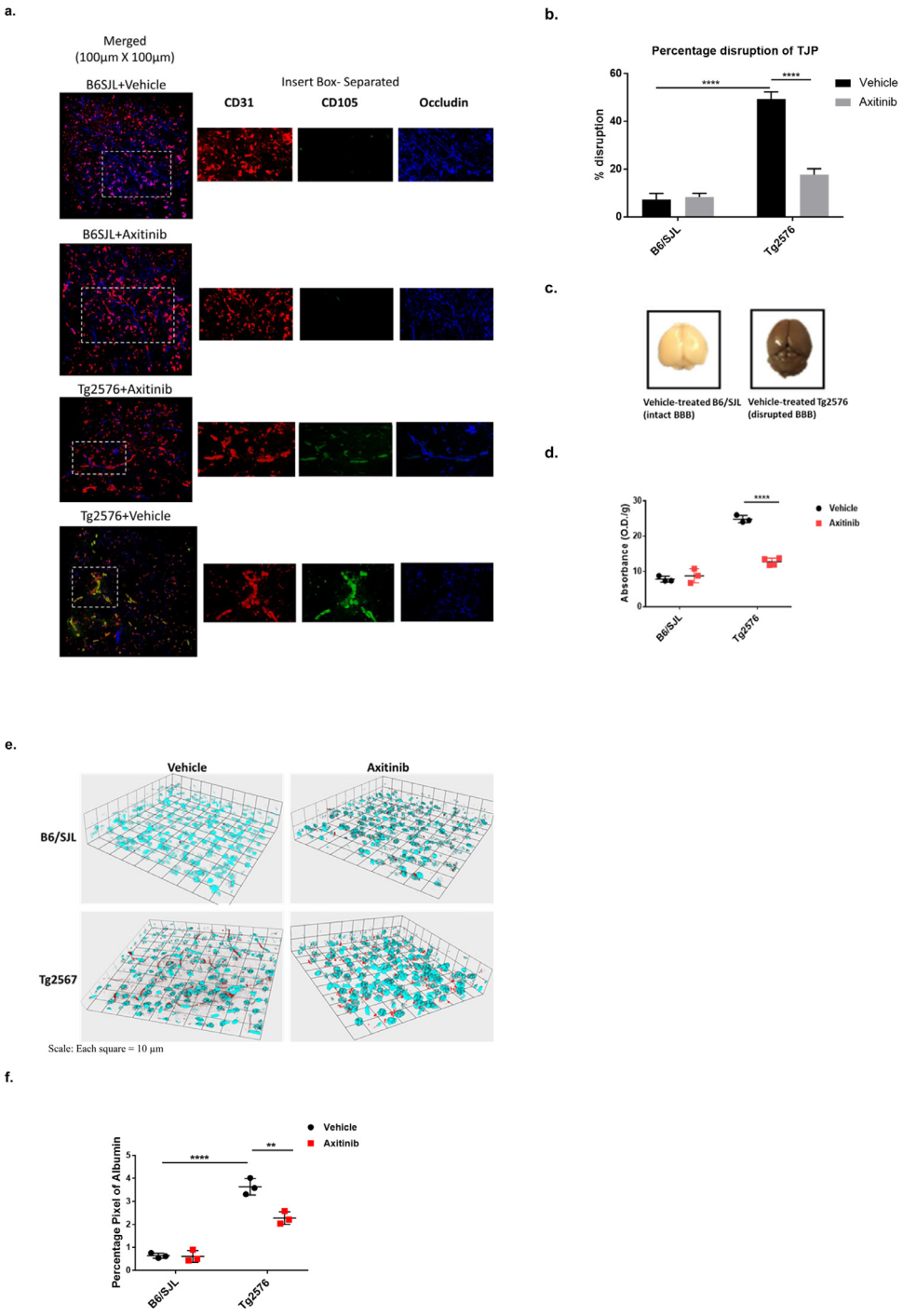

Fig. 5. Examination of tight junction proteins by immunofluorescence microscopy in the brains of Tg2576 mice and their WT littermates. **a)** Brains from perfused mice were used for immunofluorescence analysis of the BBB. Cortical brain sections were stained for the combination of markers CD105, CD31 and the tight junction protein, Occludin. Panel a) shows a micrograph of the cortical region of the brain with merged CD31 (red), CD105 (green) and Occludin (blue) staining whereas the other three panels show CD31, CD105 and Occludin where the field of view was enlarged to reveal a more detailed view of the structures. **b)** The percentage of tight junction protein disruption is shown graphically (WT B6SJL n= 5 and Tg2576 n= 6). The data are representative of three separate experiments (two-tailed unpaired t-test, * $p<0.03$; ** $p<0.002$; *** $p<0.0002$; **** $p<0.0001$). **c)** Images of the brain show an intact BBB and a disrupted BBB. Evans Blue staining is normally very low when the BBB is intact. Post-treatment with Evans Blue, the harvested brains from WT mice showed no colouration, while the brains from vehicle-treated Tg2576 mice appeared blue. **d)** Post-treatment with Evans Blue, the dye was extracted from the brains, minus the olfactory bulbs and the cerebellum. The absorbance of the extracted dye was read with an ELISA plate reader at 620 nm, and the readings were divided by the weight of the brain. An increase in the uptake of Evans Blue in the brain homogenates prepared from the vehicle-treated Tg2576 mice was indicated by the high absorbance of the dye. No difference was observed between the vehicle- and drug-treated WT (B6/SJL) mice. Axitinib treatment of the Tg2576 mice resulted in less Evans Blue staining than in the vehicle-treated animals, thereby indicating restoration of a functioning BBB. This experiment was repeated twice. (two-tailed unpaired t-test, * $p<0.03$; ** $p<0.002$; *** $p<0.0002$; **** $p<0.0001$). **e)** The cortical micrographs here show the voxels of the field of view of the imaged sections represented by the grid. The micrographs are representative of brain sections from mice from a separate experiment, where both Tg2576 and WT animals were treated with Axitinib or delivery vehicle alone, followed by staining for albumin. Red indicates immunostained albumin that has leaked into the brain and cyan indicates the cell nucleus (stained with DAPI). Axitinib treatment was associated with less albumin leakage into the brain, indicative of a more functional BBB, in contrast to the greater albumin staining in the vehicle-treated Tg2576. **f)** The quantification of Albumin is shown as the percentage of pixels in each field of view (n=3). The data are represented as the mean± standard deviation. Statistical analysis was performed using an unpaired two-tailed t-test. (* $p<0.03$; ** $p<0.002$; *** $p<0.0002$; **** $p<0.0001$).(For interpretation of the references to colour in this figure, the reader is referred to the web version of this article.)

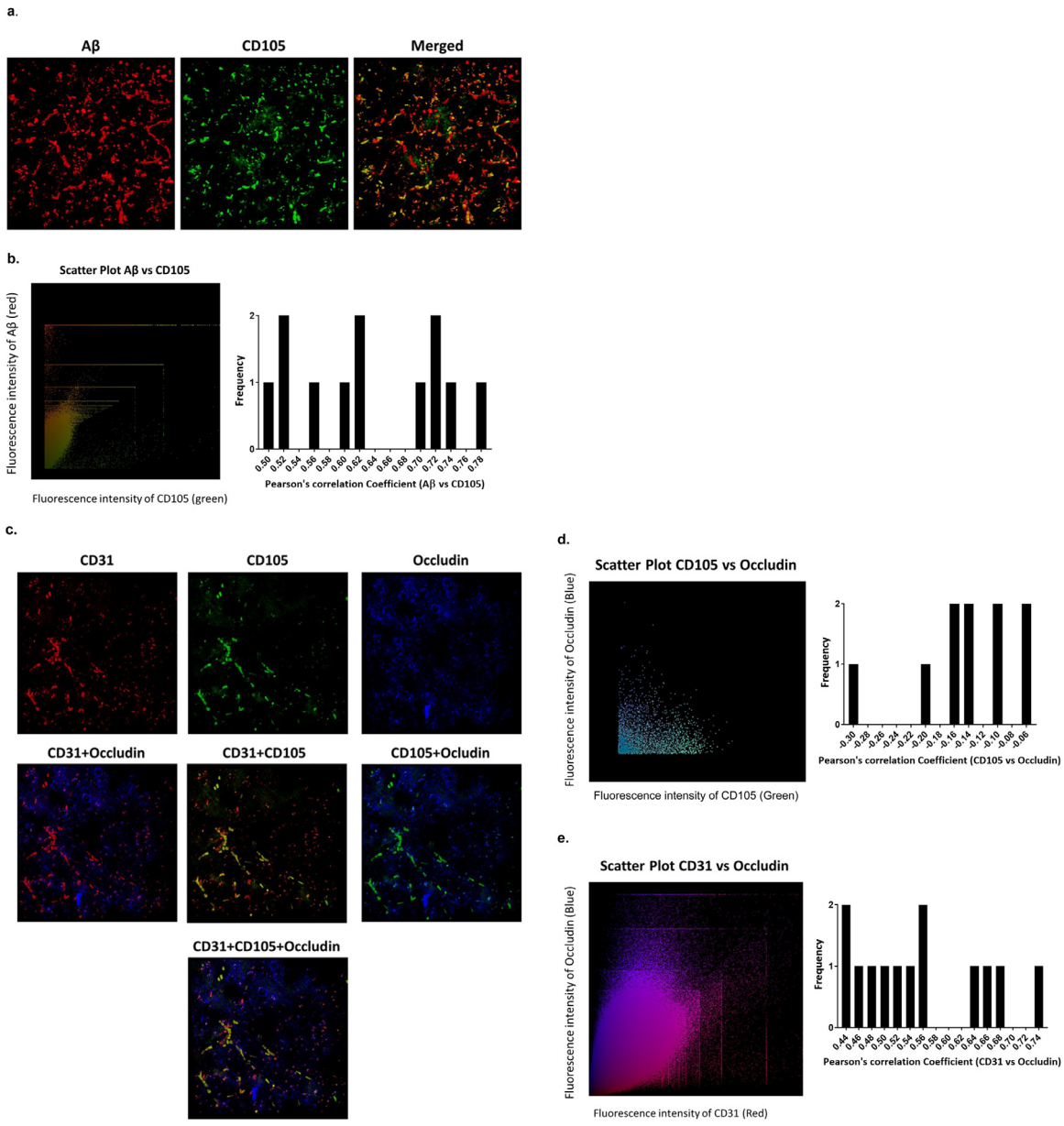

Fig. 6. Immunofluorescence colocalization of CD105 with Aβ and Occludin. **a)** Micrographs representing the cortical region of Tg2576 mouse brains depicting co-localization of CD105 and Aβ. CD105 (green), Aβ (red) and merged where Red + Green = Yellow. Size of each micrograph: 10 μm X 100 μm.**b)** The scatterplot represents the number and intensity of pixels that are plotted the merged figure (**a**) of Aβ (red) versus CD105 (green). The Thresholded Pearson's Correlation coefficients are calculated from the scatterplots of 12 separate comparisons of Aβ versus CD105 and are shown in the relative frequency histogram, for an average of (r) = +0.633 with a standard deviation of 0.096, p = 0.01 (statistically significant, one-tail t-test calculated using free statistics calculator (https://www.danielsoper.com/statcalc)). **c)** Micrographs representing cortical region of Tg2576 mouse brains depicting cosiglocalization of CD31 (red), CD105 (green), and Occludin (blue). Merged micrographs show Green + Red = Yellow; Red + Blue = Purple; Blue + Green = Cyan; and Red + Blue + Green = White. Size represented in each micrograph: 100 μm X100 μm. **d)** The scatterplot represents the number and intensity of pixels that are plotted in the merged figure for CD31 (red) vs Occludin (blue). The Thresholded Pearson's Correlation coefficients are calculated from the scatterplots of 13 separate comparisons of CD31 versus Occludin and shown in the relative frequency histogram, for an average of (r) = +0.552 with a standard deviation of 0.095, p = 0.03 (statistically significant, one-tail t-test; calculated using free statistics calculator (https://www.danielsoper.com/statcalc)). **e)** The scatterplot represents the number and intensity of pixels that are plotted in the merged figure for CD105 (green) vs Occludin (blue). The Thresholded Pearson's Correlation coefficients are calculated from the scatterplots of 10 separate comparisons of CD105 versus Occludin and shown in the relative frequency histogram, for an average of (r) = -0.140 with a standard deviation of 0.073, p = 0.34 (one-tail t-test not statistically significant (https://www.danielsoper.com/statcalc). (For interpretation of the references to colour in this figure, the reader is referred to the web version of this article.)

and other pathological indications observed in the Tg2576 mouse model of AD. This study demonstrates the proof of concept that the chemical inhibition of cerebral angiogenesis dramatically reduces neoangiogenesis, restores BBB integrity, resolves tight-junction pathogenesis, and diminishes cognitive decline in a model of AD. Axitinib binds to the intracellular tyrosine kinase catalytic domains of VEGFR1-3, PDGFR and c-KIT receptors, blocking the downstream angiogenic signalling pathways thus resulting in the reduction of AD pathology.

Therapies directed at the amyloid cascade pathway have thus far generally failed to alleviate AD pathology and restore cognition and memory. Consequently, new approaches to prevent and treat AD are urgently needed. Our earlier discovery of vascular dysfunction in AD [7,10,14,26,46] has gained traction in the field as a crucial pathological hallmark of AD. Considering the amount of time, effort and resources required to test new drugs in pre-clinical and clinical trials, demonstrating the efficacy of an already-approved drug such as Axitinib facilitates accelerating the repurposing of this drug for another

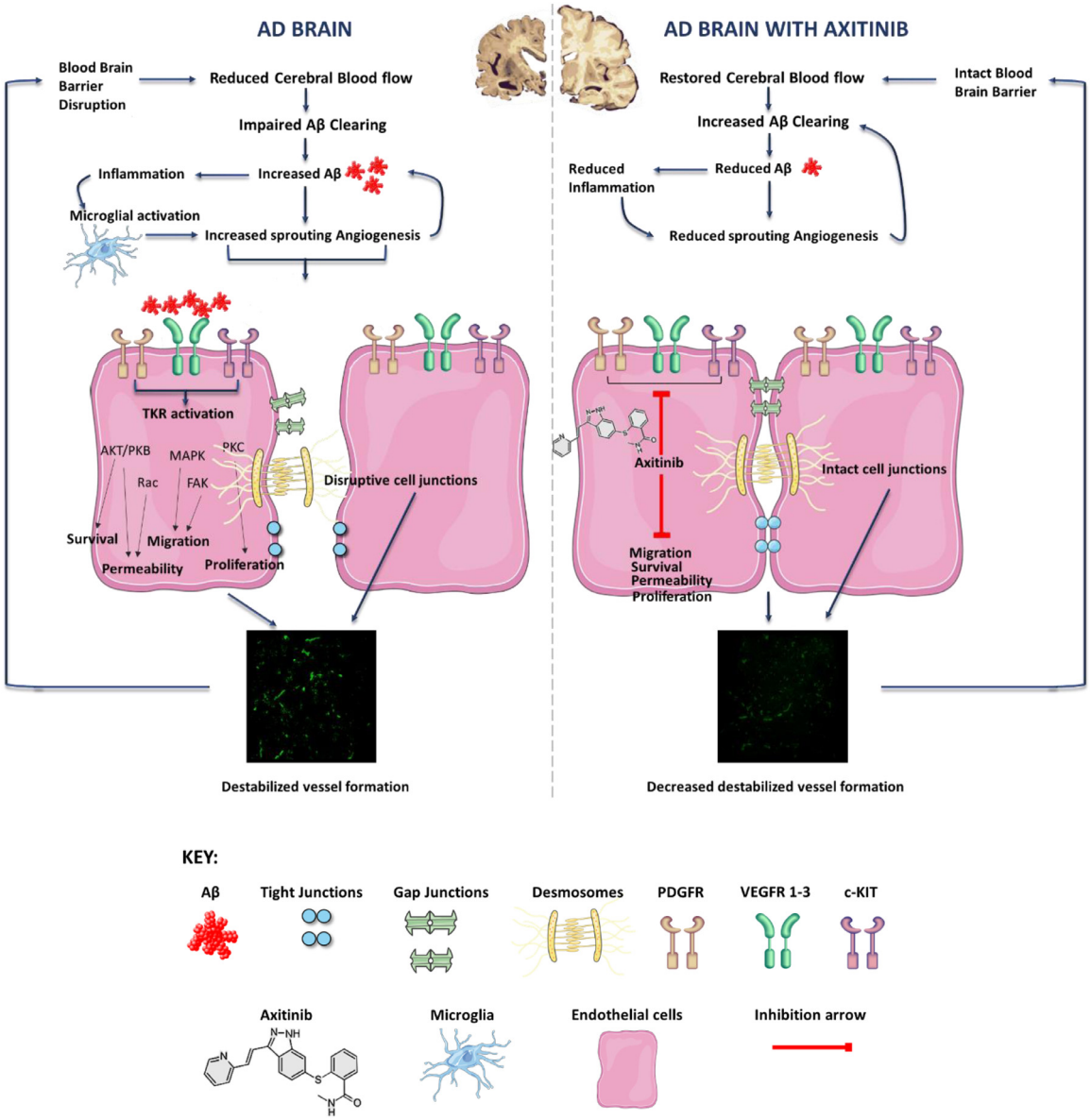

Fig. 7. Schematic depicting the mechanism of action of Axitinib as a therapeutic for Alzheimer's disease.

disease. By demonstrating reduction of pathology and reversing cognitive decline in an AD mouse model, we are cautiously optimistic that this study provides the catalyst for further investigation of this alternative approach for the treatment of devastating diseases, such as AD or CAA, which currently have very few other therapeutic options. However, we are mindful that Axitinib is a chemotherapeutic and the demographic of the target population is elderly, thus there may be issues regarding tolerability and side effects noted in cancer patients receiving treatment with Axitinib include; diarrhea, dysphonia, fatigue, anemia, hand-foot syndrome and hypertension [30,32,33]. Conversely, Axitinib has been noted to be neuroprotective, demonstrated by increasing the viability of primary mouse neuron cultures in the presence of VEGF and Aβ 1-42 [46]. Additionally, Axitinib is thought to have a superior toxicity profile compared to other tyrosine kinase inhibitors (TKIs) [34]. Future studies will be required to determine the optimum treatment modality and dosing levels required to restore BBB integrity and abate cerebral vascular neoangiogenesis in AD.

It is noteworthy that other neurological diseases have been treated with repurposed cancer drugs at low doses with great success in modulating disease progression. For example, alemtuzumab [48,49], mitoxantrone [50,51], rituximab [52–54] and others are currently being used to treat multiple sclerosis [52]. It is also of interest that the 'wet' form of AMD also exhibits similar risk factors and other parallels to AD pathogenesis reported here including abnormal blood vessels (known as choroidal neovascularization) that grow under the retina and macula. Aggregates of lipids and proteins ("drusen") associated with AMD are similar in molecular composition to amyloid beta (Aβ) plaques [55]. Treatment for AMD currently involves the use of repurposed anti-angiogenic compounds [56]. Once again, in the context of these other diseases, the new approach described here to repurpose anti-cancer drugs for modulating cerebral neoangiogenesis in AD shows considerable promise in a preclinical model and may prove efficacious in treating AD patients.

From the available data, a new mechanism emerges from this study that describes how Aβ causes pathological neoangiogenesis, disruption of tight junctions and the breakdown of the blood-brain barrier (BBB) leading to further AD pathology. In this model, depicted in Fig. 7, reduced cerebral blood flow leads to an increase in amyloidogenesis, a decrease in the clearance of Aβ which, in turn, increases

levels of Aβ observed interacting with cerebral vessels. This, along with inflammation caused by the increased levels of Aβ, activates tyrosine kinase receptors and the signalling pathways downstream, including activation of pro-angiogenic transcription factors for endothelial survival, proliferation, migration, and increased vessel permeability. This triggers increased neoneoangiogenic sprouting (demonstrated in **Fig. 6** as increased staining of vessels for CD105) and result in the formation of destabilized blood vessels. Increases in certain effector molecules, like FAK, lead to rearrangement of the actin cytoskeleton which disrupts cell junctions and the eventual disruption of the BBB. Disruption of the BBB allows toxic blood molecules to enter the central nervous system, resulting in further inflammation and the induction of hypoxia and neuronal pathology. In this way, sprouting neoangiogenesis culminates in AD pathology and contributes to cognitive decline. In contrast, when the AD brain is treated with the tyrosine kinase inhibitor, Axitinib, the downstream signaling pathways that induce destabilized vessel formation is blocked and the overall angiogenesis is reduced. The restoration of tight cell junctions decreases the permeability of the BBB and improves cerebral blood flow, which promotes clearing of the Aβ. This leads to a reduction of inflammation and a reduction in the release of pro-angiogenic signals. With an intact BBB, CNS damage is ameliorated and healthy brain function can resume. This study illustrates that treatment with Axitinib improves cognition, memory and behaviour of the aged Tg2576 mice that previously exhibited signs of dementia. Future studies addressing the prophylactic treatment of Tg2576 AD mice (*i.e.* before pathology or abnormal behaviour becomes apparent) will answer the question of whether Axitinib treatment can forestall the pathogenesis and progression of cognitive decline in AD.

Caveats and limitations:

Understanding new aspects of the pathophysiology of AD pathogenenesis leads to new therapeutic opportunities for treating dementia. We describe a new therapeutic approach that directly repurposes the use of anti-cancer drugs to modulate cerebral neoangiogenesis, and that may prove effective in treating AD and related vascular diseases of the brain. However, Axitinib is a cancer therapeutic, that may have side effects and tolerability issues, especially considering the target demographic is the aged and this treatment is projected to be administered over an extended period of time. Furthermore, although Axitinib is a second-generation TKI that is more specific and possesses lower toxicity than other TKIs in cancer patients, dosing will need to be addressed in future clinical trials for treating AD. The need to expand research on this therapeutic modality and to clinically translate the approach described in this study remains a priority and a challenge for future studies.

5. Author's contributions

WAJ: conceived idea. CSBS and WAJ: designed research. CSBS, KBC, LM, HYW: performed research. CSBS, CGP and WAJ: analyzed data. CSBS and WAJ: wrote paper. CSBS, LM, CGP and WAJ: edited paper.

Declaration of Competing Interest

CSBS is an inventor on a patent licensed to Cava Healthcare Inc. KBC has nothing to disclose. LM reports receiving personal fees from Cava Healthcare, Inc. HYW has nothing to disclose. CGP reports personal fees from Cava Healthcare Inc., and is a consultant to Cava Healthcare Inc. WAJ is an inventor on a related patent and received fees and became a director of Cava Healthcare, Inc. subsequent to the completion of this study.

Data sharing statement

The authors acknowledge that the data presented in this study can be found in the supplementary information.

Acknowledgments

Funding: CSBS was the recipient of a UBC Centre for Blood Research Graduate Student Award and the William and Dorothy Gilbert Graduate Scholarship in Biomedical Sciences ; WAJ was supported by grants from the Canadian Institutes of Health Research (MOP-133635) and by the W. Garfield Weston Foundation (RR161038). The funding sources had no role in the study design, data collection, analysis or interpretation of data, or in the writing of the paper. The authors wish to acknowledge the very helpful editorial comments on this manuscript by Professor Terry W. Pearson (University of Victoria).

Supplementary materials

Supplementary material associated with this article can be found in the online version at doi:10.1016/j.ebiom.2021.103503.

References

[1] Greenberg SM, Bacskai BJ, Hernandez-Guillamon M, et al. Cerebral amyloid angiopathy and Alzheimer disease – one peptide, two pathways. Nat Rev Neurol 2020;16:30–42. doi: 10.1038/s41582-019-0281-2.
[2] Cummings J, Lee G, Ritter A, Zhong K. Alzheimer's disease drug development pipeline: 2018. Alzheimers Dement 2018;4:195–214 (N Y).
[3] Cummings J. Drug development for psychotropic, cognitive-enhancing, and disease-modifying treatments for Alzheimer's disease. J Neuropsychiatry Clin Neurosci 2020:appineuropsych20060152.
[4] Mehta D, Jackson R, Paul G, Shi J, Sabbagh M. Why do trials for Alzheimer's disease drugs keep failing? A discontinued drug perspective for 2010-2015. Expert Opin Investig Drugs 2017;26(6):735–9.
[5] Cummings JL, Morstorf T, Zhong K. Alzheimer's disease drug-development pipeline: few candidates, frequent failures. Alzheimers Res Ther 2014;6(4):37.
[6] Scott TJ, O'Connor AC, Link AN, Beaulieu TJ. Economic analysis of opportunities to accelerate Alzheimer's disease research and development. Ann N Y Acad Sci 2014;1313:17–34.
[7] Biron KE, Dickstein DL, Gopaul R, Jefferies WA. Amyloid triggers extensive cerebral angiogenesis causing blood brain barrier permeability and hypervascularity in Alzheimer's disease. Plos One 2011;6(8):e23789.
[8] Claassen JA, Zhang R. Cerebral autoregulation in Alzheimer's disease. J Cereb Blood Flow Metab 2011;31(7):1572–7.
[9] Pfeifer M, Boncristiano S, Bondolfi L, Stalder A, Deller T, Staufenbiel M, et al. Cerebral hemorrhage after passive anti-Abeta immunotherapy. Science 2002;298(5597):1379.
[10] Ujiie M, Dickstein D, Carlow D, Jefferies WA. Blood-brain barrier permeability precedes senile plaque formation in an Alzheimer disease model. Microcirculation 2003;10:463–70.
[11] Dickstein DL, Walsh J, Brautigam H, Stockton SD,Jr, Gandy S, Hof PR. Role of vascular risk factors and vascular dysfunction in Alzheimer's disease. Mt Sinai J Med. 2010;77(1):82–102.
[12] Dickstein DL, Biron KE, Ujiie M, Pfeifer CG, Jeffries AR, Jefferies WA. A{beta} peptide immunization restores blood-brain barrier integrity in Alzheimer disease. Faseb J 2006;20(3):426–33.
[13] Dickie BR, Vandesquille M, Ulloa J, Boutin H, Parkes LM, Parker GJM. Water-exchange MRI detects subtle blood-brain barrier breakdown in Alzheimer's disease rats. Neuroimage 2019;184:349–58.
[14] Biron KE, Dickstein DL, Gopaul R, Fenninger F, Jefferies WA. Cessation of Neoangiogenesis in Alzheimer's Disease Follows Amyloid-beta Immunization. Sci Rep 2013;3:1354.
[15] Singh C, Pfeifer CG, Jefferies WA. Pathogenic angiogenic mechanisms in Alzheimer's disease: Chapter 6. InTechOpen; 2017 Simionescu D, editor:.
[16] Vinters HV. Cerebral amyloid angiopathy. A critical review. Stroke 1987;18(2):311–24.
[17] Holton JL, Ghiso J, Lashley T, Rostagno A, Guerin CJ, Gibb G, et al. Regional distribution of amyloid-Bri deposition and its association with neurofibrillary degeneration in familial British dementia. Am J Pathol 2001;158(2):515–26.
[18] Richard E, Carrano A, Hoozemans JJ, van Horssen J, van Haastert ES, Eurelings LS, et al. Characteristics of dyshoric capillary cerebral amyloid angiopathy. J Neuropathol Exp Neurol 2010;69(11):1158–67.
[19] Jellinger KA. The enigma of vascular cognitive disorder and vascular dementia. Acta Neuropathol 2007;113(4):349–88.
[20] Ruitenberg A, den Heijer T, Bakker SL, van Swieten JC, Koudstaal PJ, Hofman A, et al. Cerebral hypoperfusion and clinical onset of dementia: the Rotterdam Study. Ann Neurol 2005;57(6):789–94.

[21] Vagnucci AH, Li WW. Alzheimer's disease and angiogenesis. Lancet 2003;361 (9357):605–8.
[22] Kara F, Dongen ES, Schliebs R, Buchem MA, Groot HJ, Alia A. Monitoring blood flow alterations in the Tg2576 mouse model of Alzheimer's disease by in vivo magnetic resonance angiography at 17.6 T. Neuroimage 2012;60 (2):958–66.
[23] Thal DR, Capetillo-Zarate E, Larionov S, Staufenbiel M, Zurbruegg S, Beckmann N. Capillary cerebral amyloid angiopathy is associated with vessel occlusion and cerebral blood flow disturbances. Neurobiol Aging 2009;30(12):1936–48.
[24] Pfeifer LA, White LR, Ross GW, Petrovitch H, Launer LJ. Cerebral amyloid angiopathy and cognitive function: the HAAS autopsy study. Neurology 2002;58 (11):1629–34.
[25] Sweeney MD, Montagne A, Sagare AP, Nation DA, Schneider LS, Chui HC, et al. Vascular dysfunction-The disregarded partner of Alzheimer's disease. Alzheimers Dement 2019;15(1):158–67.
[26] Jefferies WA, Price KA, Biron KE, Fenninger F, Pfeifer CG, Dickstein DL. Adjusting the compass: new insights into the role of angiogenesis in Alzheimer's disease. Alzheimers Res Ther 2013;5(6):64.
[27] Desai BS, Schneider JA, Li JL, Carvey PM, Hendey B. Evidence of angiogenic vessels in Alzheimer's disease. J Neural Transm 2009;116(5):587–97.
[28] Zlokovic BV. Neurovascular pathways to neurodegeneration in Alzheimer's disease and other disorders. Nat Rev Neurosci 2011;12(12):723–38.
[29] Iadecola C. Neurovascular regulation in the normal brain and in Alzheimer's disease. Nat Rev Neurosci 2004;5(5):347–60.
[30] Rini BI, Escudier B, Tomczak P, Kaprin A, Szczylik C, Hutson TE, et al. Comparative effectiveness of axitinib versus sorafenib in advanced renal cell carcinoma (AXIS): a randomised phase 3 trial. Lancet 2011;378(9807):1931–9.
[31] Gross-Goupil M, Francois L, Quivy A, Ravaud A. Axitinib: a review of its safety and efficacy in the treatment of adults with advanced renal cell carcinoma. Clin Med Insights Oncol 2013;7:269–77.
[32] Gross-Goupil M, Kwon TG, Eto M, Ye D, Miyake H, Seo SI, et al. Axitinib versus placebo as an adjuvant treatment of renal cell carcinoma: results from the phase III, randomized ATLAS trial. Ann Oncol 2018;29(12):2371–8.
[33] Tomita Y, Uemura H, Oya M, Shinohara N, Habuchi T, Fujii Y, et al. Patients with metastatic renal cell carcinoma who benefit from axitinib dose titration: analysis from a randomised, double-blind phase II study. BMC Cancer 2019;19(1):17.
[34] Albiges L, Izzedine H, Ederhy S, Robert C, Gravis G, Boyle H, et al. [Axitinib in metastatic renal carcinomas: update of knowledge about side effects]. Bull Cancer 2014;101(10):976–88.
[35] Hsiao K, Chapman P, Nilsen S, Eckman C, Harigaya Y, Younkin S, et al. Correlative memory deficits, Abeta elevation, and amyloid plaques in transgenic mice. Science 1996;274(5284):99–102.
[36] Westerman MA, Cooper-Blacketer D, Mariash A, Kotilinek L, Kawarabayashi T, Younkin LH, et al. The relationship between Abeta and memory in the Tg2576 mouse model of Alzheimer's disease. J Neurosci 2002;22(5):1858–67.
[37] Stewart S, Cacucci F, Lever C. Which memory task for my mouse? A systematic review of spatial memory performance in the Tg2576 Alzheimer's mouse model. J Alzheimers Dis 2011;26(1):105–26.
[38] van de Haar HJ, Burgmans S, Jansen JF, van Osch MJ, van Buchem MA, Muller M, et al. Blood-brain barrier leakage in patients with early Alzheimer disease. Radiology 2016;281(2):527–35.
[39] Nation DA, Sweeney MD, Montagne A, Sagare AP, D'Orazio LM, Pachicano M, et al. Blood-brain barrier breakdown is an early biomarker of human cognitive dysfunction. Nat Med 2019;25(2):270–6.
[40] Hsiao KK, Borchelt DR, Olson K, Johannsdottir R, Kitt C, Yunis W, et al. Age-related CNS disorder and early death in transgenic FVB/N mice overexpressing Alzheimer amyloid precursor proteins. Neuron 1995;15(5):1203–18.
[41] Hofling C, Morawski M, Zeitschel U, Zanier ER, Moschke K, Serdaroglu A, et al. Differential transgene expression patterns in Alzheimer mouse models revealed by novel human amyloid precursor protein-specific antibodies. Aging Cell 2016;15 (5):953–63.
[42] Radu M, Chernoff J. An *in vivo* assay to test blood vessel permeability. J Vis Exp 2013(73):e50062.
[43] Rugo HS, Herbst RS, Liu G, Park JW, Kies MS, Steinfeldt HM, et al. Phase I trial of the oral antiangiogenesis agent AG-013736 in patients with advanced solid tumors: pharmacokinetic and clinical results. J Clin Oncol 2005;23(24):5474–83.
[44] Hu-Lowe DD, Zou HY, Grazzini ML, Hallin ME, Wickman GR, Amundson K, et al. Nonclinical antiangiogenesis and antitumor activities of axitinib (AG-013736), an oral, potent, and selective inhibitor of vascular endothelial growth factor receptor tyrosine kinases 1, 2, 3. Clin Cancer Res 2008;14(22):7272–83.
[45] De Spiegelaere W, Casteleyn C, Van den Broeck W, Plendl J, Bahramsoltani M, Simoens P, et al. Intussusceptive angiogenesis: A biologically relevant rorm of angiogenesis. J Vascular Res 2012;49(5):390–404.
[46] Dickstein D, Jefferies W, editors. The relationship of activated microglia to amyloid accumulation in Alzheimer disease. Elsevier Science Inc; 2002. Neurobiol Aging;360 Park Ave South, New York, NY 10010-1710 USA.
[47] Wood LB, Winslow AR, Proctor EA, McGuone D, Mordes DA, Frosch MP, et al. Identification of neurotoxic cytokines by profiling Alzheimer's disease tissues and neuron culture viability screening. Sci Rep 2015;5:16622.
[48] Fraser G, Smith CA, Imrie K, Meyer R. Hematology disease site groupof cancer care ontario's program in evidence-based C. Alemtuzumab in chronic lymphocytic leukemia. Curr Oncol 2007;14(3):96–109.
[49] Berger T, Elovaara I, Fredrikson S, McGuigan C, Moiola L, Myhr KM, et al. Alemtuzumab use in clinical practice: recommendations from European multiple sclerosis experts. CNS Drugs 2017;31(1):33–50.
[50] Chartier N, Epstein J, Soudant M, Dahan C, Michaud M, Pittion-Vouyovitch S, et al. Clinical follow-up of 411 patients with relapsing and progressive multiple sclerosis 10 years after discontinuing mitoxantrone treatment: a real-life cohort study. Eur J Neurol 2018;25(12):1439–45.
[51] Faulds D, Balfour JA, Chrisp P, Mitoxantrone LHD. A review of its pharmacodynamic and pharmacokinetic properties, and therapeutic potential in the chemotherapy of cancer. Drugs 1991;41(3):400–49.
[52] Kieseier BC, Jeffery DR. Chemotherapeutics in the treatment of multiple sclerosis. Ther Adv Neurol Disord 2010;3(5):277–91.
[53] Salles G, Barrett M, Foa R, Maurer J, O'Brien S, Valente N, et al. Rituximab in B-cell hematologic malignancies: a review of 20 years of clinical experience. Adv Ther 2017;34(10):2232–73.
[54] Castillo-Trivino T, Braithwaite D, Bacchetti P, Waubant E. Rituximab in relapsing and progressive forms of multiple sclerosis: a systematic review. Plos One 2013;8 (7):e66308.
[55] Mullins RF, Russell SR, Anderson DH, Hageman GS. Drusen associated with aging and age-related macular degeneration contain proteins common to extracellular deposits associated with atherosclerosis, elastosis, amyloidosis, and dense deposit disease. Faseb J 2000;14(7):835–46.
[56] Tzoumas N, Hallam D, Harris CL, Lako M, Kavanagh D, Steel DHW. Revisiting the role of factor H in age-related macular degeneration: insights from complement-mediated renal disease and rare genetic variants. Surv Ophthalmol 2021;66 (2):378–401.